High-Dynamic Frequency Tracking Using Wavelets

K. Hamdan, H. Tsou, and S. M. Hinedi
Communications Systems and Research Section

In this article, we investigate the use of wavelets for frequency tracking in the presence of high dynamics. In particular, we construct automatic frequency control loops that are based on correlating the incoming sinusoidal signal with Fourier-based functions and with Daubechies-4 wavelet functions. Both loops are compared based on their abilities to track an input frequency with varying degrees of frequency rate. For each loop, we show the steady-state frequency error and corresponding steady-state variance as a function of the frequency rate of the input signal. The results indicate that when the input frequency rate is close to zero (nearly constant frequency input), the Fourier-based loop achieves lower variance than does the wavelet-based loop. As the frequency rate increases (high dynamics), the performance of the Fourier-based loop degrades, and ultimately the Fourier-based loop ceases to track. Meanwhile, the wavelet-based loop achieves a lower steady-state error and continues to successfully track in frequency rate ranges where the Fourier-based loop breaks down. Thus, this study suggests that wavelets can be a viable alternative to traditional Fourier-based frequency tracking loops when the input is undergoing high dynamics. This type of dynamics could be found in applications such as space probes descending through a turbulent and unpredictable planetary atmosphere. However, during normal spacecraft cruise, more traditional Fourier-based loops will outperform wavelet-based loops.

I. Introduction

In coherent communications systems, automatic frequency control (AFC) loops often are used for initial frequency acquisition and subsequent tracking of modulated and unmodulated sinusoidal signals. When the signal is corrupted by additive Gaussian white noise, frequency tracking is accomplished by adaptively estimating the frequency using a variety of estimation techniques. Traditionally, frequency estimation procedures are based on the maximum a priori (MAP) method, which is based on correlating the incoming signal with an appropriately chosen set of orthonormal functions. In an open-loop setting, the MAP estimate is equated to the discrete frequency corresponding to the sinusoid with which the received signal achieves maximum correlation. For complex sinusoidal signals with constant frequency and additive white noise, the best basis [in the sense of maximizing the signal-to-noise ratio (SNR)] is the Fourier basis. This represents the "matched filter" in the sense that the incoming signal has the same form as the basis functions. Closed-loop variants of this method involve adjusting the frequency of a locally generated oscillator (NCO) so as to minimize the frequency of an error signal whose frequency corresponds to the difference between the frequency of the received signal and that of the NCO. Thus, when the frequency of the error signal is sufficiently small, as it is in the tracking mode, the MAP frequency estimate of the received signal is equated to the frequency of the NCO. Alternatively, suboptimal closed-

loop procedures, such as the differentiator and cross-product AFC [1], adjust the frequency of the NCO so as to minimize (in absolute value) the discrete derivative of the spectrum of the incoming signal.

In principle, the MAP method and its variants assume that the frequency is constant during the observation interval. In particular, the Fourier-based AFC loop would be optimal (in the sense of reducing jitter) when the frequency is constant. When the incoming signal is undergoing high dynamics, such as those transmitted by probes during their descents into unpredictable planetary atmospheres, the Fourier spectrum of the signal undergoes smearing and, hence, the Fourier basis may not be the optimal basis. This is in fact the dilemma faced by a Fourier-based estimation scheme: On the one hand, a shorter integration time (or, equivalently, observation window) is required to reduce the smearing caused by high dynamics. On the other hand, a longer integration time is required to raise the detection SNR. Thus, as will be shown in some examples, if the dynamics are high enough and the SNR low enough, a Fourier-based AFC loop with a fixed observation window eventually will break down.

As a possible remedy to the above problem, a wavelet-based AFC loop is considered in this article. The main feature of wavelets that can make them advantageous for spectral analysis is the fact that high-frequency components require shorter integration times than do low-frequency components. As a result, increasing the observation window does not introduce a major smearing effect, as it does for a Fourier-based loop. Indeed, we will show that the wavelet-based open-loop variance at high frequencies is not affected by the size of the observation window. Consequently, when the signal is undergoing high dynamics, reducing the observation window does not increase the variance of the frequency error provided it is large enough. Moreover, because large frequency components can be estimated using shorter integration times, we can obtain large frequency errors much faster by using a wavelet-based loop than we would by using a Fourier-based loop. This is an important advantage when considering frequency acquisition issues. However, there are two disadvantages associated with wavelets. First, a wavelet-based loop is more difficult to implement than the well-understood Fourier-based loop. Second, when the frequency is constant, leading to small frequency errors, longer integration times are required. Hence, reducing the observation interval can increase the variance at low frequencies. In fact, for the constant input case, the wavelet basis does not represent the matched filter and, thus, the Fourier-based loop achieves lower variance than the wavelet-based loop. Thus, what we would expect (and what this investigation will confirm) is that wavelet-based AFC loops are better at tracking a signal when the frequency rate is large. This would be useful for tracking a probe that is descending through a planetary atmosphere, such as at Jupiter. In this case, the dynamics would be very large and unpredictable and a Fourier-based loop might not be able to track the signal. However, when the frequency is constant or completely predictable, such as the case during normal spacecraft cruise, more traditional Fourier-based loops perform better than do wavelet-based loops.

In [2], frequency tracking loops based on short-time discrete Fourier transform and Harr wavelet functions were compared. Only constant-frequency input signals were considered. The purpose of this article is to extend the analysis to the variable input case and further investigate the above ideas more concretely. In particular, we consider the use of wavelets in an AFC loop in the presence of high dynamics and compare the results with Fourier-basis functions. Although the approach used in this article will be valid for any wavelet family, the Daubechies-4 (D4) wavelet was chosen here because of its desirable properties. It is compactly supported with a power spectrum that exhibits a single clear peak with small side lobes. In Section II, we present the general setting and also describe the general form of the AFC loops to be considered. In order to verify the simulation examples, in Section III we develop a generic theory that predicts the open-loop performance of MAP-based AFC loops based on any orthonormal basis. In Section IV, this theory is confirmed with simulations using D4 wavelets and Fourier basis functions. In Section V, we investigate and compare the tracking behavior of the closed loops with a high frequency rate.

II. General AFC Loop Structure

The AFC loops to be considered in this article will have the graphical representation given in Fig. 1. The complex tone signal to be tracked is given by $r(t) = A\exp(2\pi j f_c t)$, where f_c is the unknown frequency. After the received signal is passed through a rectangular bandpass filter (BPF), we obtain the input signal to the AFC loop:

$$s(t) = r(t) + n(t) \tag{1}$$

where $n(t)$ is a zero-mean complex white Gaussian noise process with power spectral density (PSD) N_0. The input signal is mixed with the NCO signal at frequency f_o, and the result is passed through a lowpass filter (LPF) to produce the complex error signal $z(t) = I(t) + jQ(t)$, where the in-phase component, $I(t)$, is given by

$$I(t) = A\cos(2\pi f_e t) + x_n(t)\cos(2\pi f_e t) - y_n(t)\sin(2\pi f_e t) \tag{2}$$

and the quadrature component, $Q(t)$, is defined by

$$Q(t) = A\sin(2\pi f_e t) + x_n(t)\sin(2\pi f_e t) + y_n(t)\cos(2\pi f_e t) \tag{3}$$

where $x_n(t)$ and $y_n(t)$ are the baseband quadrature components of $n(t)$, each having PSD N_0, and f_e is the frequency error, defined as

$$f_e = f_c - f_o \tag{4}$$

The error signal, $z(t)$, is then passed through a spectrum analyzer, which is assumed to be based on projecting the error signal onto a set $\{\psi_1, \cdots, \psi_M, \psi_1^*, \cdots, \psi_M^*\}$ of $2M$ complex orthonormal basis functions for a duration of T seconds. The resultant projection coefficients are then used in a detection algorithm aimed at estimating the error frequency, $f_e(t)$. In discrete time, the frequency of the NCO is updated at time $k+1$ using the recursion

$$f_o(k+1) = f_o(k) + G(\hat{f}_e(k)) \tag{5}$$

where G is an operator representing the loop filter (LF) and $\hat{f}_e(k)$ is the estimate of the true frequency error, $f_e(k)$.

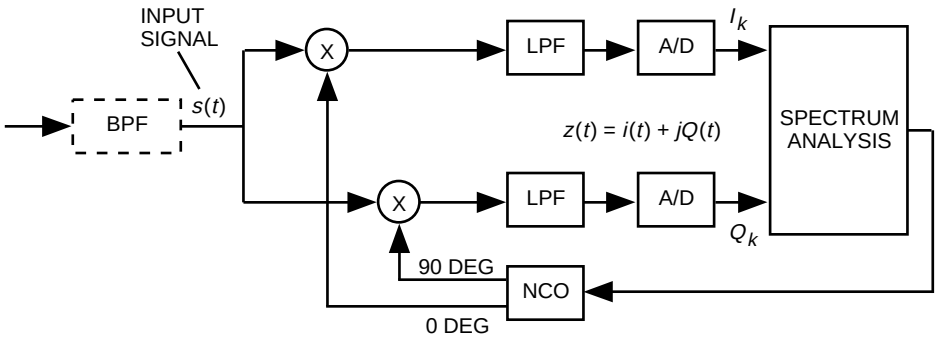

Fig. 1. Feed-back type of AFC loop.

In order to analyze the steady-state behavior of Eq. (5), we will obtain a probability density function (PDF) for the random process $\hat{f}_e(k)$ conditioned on $f_e(k)$, which ultimately will depend on the basis functions $\{\psi_n\}$ and the detection algorithm. A subsequent open-loop analysis assuming constant frequency input will help us analyze the closed loop in the presence of high dynamics.

III. Open-Loop Analysis

We assume that a function $\psi_n(t)$ belonging to the basis set is of the form

$$\psi_n(t) = \psi_{nR}(t) + j\psi_{nI}(t) \tag{6}$$

where the real-valued function $\psi_{nR}(t)$ is orthogonal to the real-valued function $\psi_{mI}(t)$ over the interval $[0, T]$ in the sense that

$$\langle \psi_{nR}, \psi_{mI} \rangle = \int_0^T \psi_{nR}(t)\psi_{mI}(t)dt = 0 \quad 1 \leq m, n \leq M \tag{7}$$

and that each set $\{\psi_{nR}\}$ and $\{\psi_{nI}\}$, $n = 1, \cdots, M$ forms an orthonormal set under the inner product defined by Eq. (7). It follows immediately that the set $\{\psi_n\}$ forms an orthonormal basis with respect to the inner product defined by

$$\langle s(t), g(t) \rangle = \int_0^T s(t)g^*(t)dt \tag{8}$$

where $s(t)$ and $g(t)$ are complex valued. Let c_n^+ and c_n^- be defined by

$$\left.\begin{aligned} c_n^+ &= \langle z(t), \psi_n(t) \rangle \\ c_n^- &= \langle z(t), \psi_n^*(t) \rangle \end{aligned}\right\} \tag{9}$$

where $z(t)$ is the error signal with in-phase and quadrature components defined in Eqs. (2) and (3). With the error frequency f_e fixed, the following are easily shown (e.g, [3]):

(1) Both c_n^+ and c_n^- are complex Gaussian random variables with real and imaginary parts having variance $\sigma^2 = N_0$, and their respective means are given by

$$\mu_n^+ = \langle s_e(t), \psi_n(t) \rangle$$

and

$$\mu_n^- = \langle s_e(t), \psi_n^*(t) \rangle$$

where $s_e(t) = A\exp(2\pi j f_e t)$.

(2) Let $g_n^+ = |c_n^+|$ and $g_n^- = |c_n^-|$. Following arguments similar to those in [3], we can show that g_n^+ is Rician with a PDF of

$$f(g_n^+) = I_0\left(\frac{g_n^+}{\sigma^2}|\mu_n^+|\right)\frac{g_n^+}{\sigma^2}\exp\left(\frac{-({g_n^+}^2 + |\mu_n^+|^2)}{2\sigma^2}\right) \tag{10}$$

where $I_0(x)$ is the zeroth-order modified Bessel function and g_n^- is also Rician with the mean $|\mu_n^-|$ replacing $|\mu_n^+|$ in Eq. (10).

(3) The g_n^+ is independent and uncorrelated with g_m^+ for $m \neq n$ and is independent and uncorrelated with g_m^- for all m. We note here that the uncorrelation property follows from the orthogonality of the basis functions.

From the above properties, we can derive a PDF of the error frequency estimate, $\hat{f}_e$, conditioned on the true error, f_e. But first, we must assume a loop filter G and a detection algorithm. When the input frequency is constant, we may assume the loop filter is simply a gain, g . The detection algorithm we assume is maximum a priori (MAP). In this case, the error estimate, $\hat{f}_e$, is set to the frequency that corresponds to the maximum component of the vector $\mathcal{G} = (g_1^+, \cdots, g_M^+, g_1^-, \cdots g_M^-)$. In other words,

$$\hat{f}_e = \sum_{n=1}^{M} f_n^+ \hat{g_n^+} + \sum_{n=1}^{M} f_n^- \hat{g_n^-} \tag{11}$$

where $f_n^+ (f_n^- = -f_n^+)$ is the frequency associated with the coefficient $g_n^+(g_n^-)$, and $\hat{g_n^+}(\hat{g_n^-})$ is 1 if $g_n^+(g_n^-)$ is the maximum component of the vector $\mathcal{G}$ and otherwise is zero. For simplicity, we redefine each of the $2M$ components of the vector $\mathcal{G}$ as g_n, with corresponding frequency f_n, and we express Eq. (11) simply as

$$\hat{f}_e = \sum_{n=1}^{2M} f_n \hat{g_n} \tag{12}$$

where $\hat{g_n} = 1$ if $\{g_n \geq g_m \ \forall m\}$ and 0 otherwise. Given the true error, f_e, it follows from Eq. (12) that $\hat{f}_e$ takes on the value f_n with probability p_n, where

$$p_n = P[g_n \geq g_m,\ 1 \leq m \leq 2M] = \int_0^\infty f_n(g_n)\left(\prod_{m\neq n}^{2M-1}\int_0^{g_n} f_m(g_m)dg_m\right)dg_n \tag{13}$$

where f_m, the PDF of g_m, is of the form given in Eq. (10). The S-curve and variance curve for this estimator are obtained by computing the expectation and variance of $\hat{f}_e$, respectively:

$$S(f_e) = \ : E\left(\hat{f}_e|f_e\right) = \sum_{n=1}^{2M} f_n p_n \tag{14}$$

$$\sigma_n^2 = \ : \ \text{var}\ \left(\hat{f}_e|f_e\right) = \sum_{n=1}^{2M} f_n^2 p_n - (E(\hat{f}_e|f_e))^2 \tag{15}$$

Note that, if we let the effective noise process $n_e(f_e) = \hat{f}_e - S(f_e)$, then $n_e(f_e)$ is a zero-mean process with variance given by Eq. (15).

IV. Wavelet Basis

The previous results apply to any orthonormal basis functions. In this section, we will specialize the results to D4 wavelets and then compare the results to standard Fourier basis functions. Here, we only summarize the basic definitions of wavelets. A good introduction to wavelets can be found in [4]. Procedures for constructing Daubechies wavelets can be found in [5].

We begin with real-valued wavelets. The real-valued wavelets considered here take the form

$$\psi^R_{n,k}(t) = 2^{-(n/2)}\psi^R(2^{-n}t - k) \;\; t \in R \tag{16}$$

where $\psi^R(t)$ is referred to as a mother wavelet. Thus, $\psi^R_{n,k}(t)$ is simply a scaling and translation of the mother wavelet, $\psi^R(t)$. Typically, $\psi^R_{n,k}(t)$ has a significant frequency component at frequency $f = \pm 2^{-n}$, and its support is near $t = 2^n k$. Thus, the projection coefficient of a real-valued signal onto $\psi^R_{n,k}(t)$ represents the signal component at time $t = 2^n k$ and frequency $f = \pm 2^n$. In this sense, a wavelet expansion of a nonstationary signal decomposes the signal into a time–frequency plane. Such a decomposition becomes very useful for estimating a time-varying frequency profile of a signal. In the context of frequency tracking, we require complex-valued basis functions so that positive frequencies can be distinguished from negative frequencies. We accomplish this by defining the function $\psi^I(t)$, which is the Hilbert transform of $\psi^R(t)$, and we define the complex-valued mother wavelet, $\psi(t) = \psi^R(t) + j\psi^I(t)$. Finally, the complex-valued basis functions are defined as

$$\psi_{n,k}(t) = \psi^R_{n,k}(t) + j\psi^I_{n,k}(t) \tag{17}$$

where $\psi^I_{n,k}(t)$ is a scaling and translation of $\psi^I(t)$ as in Eq. (16). For D4 wavelets, the real and imaginary parts of the mother wavelet are shown in Figs. 2 and 3, while the power spectrum of the complex-valued mother wavelet is shown in Fig. 4. Note that the support of the mother wavelet is [0,3]. It follows immediately from the definition that the support of the wavelet $\psi_{n,k}(t)$ is $[2^n k, 2^n(k+3)]$, and, as mentioned earlier, this function has a corresponding frequency component at $f = 2^{-n}$ (its complex conjugate has a component at $f = -2^{-n}$). In particular, the Fourier transform amplitude of $\psi_{n,k}$ is given

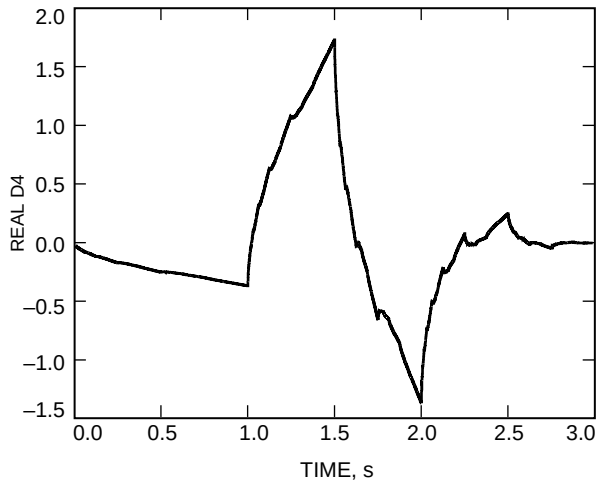

Fig. 2. The real part of D4.

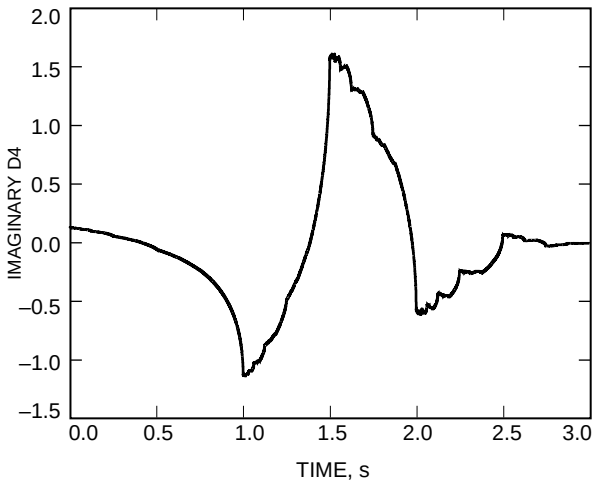

Fig. 3. The imaginary part of D4.

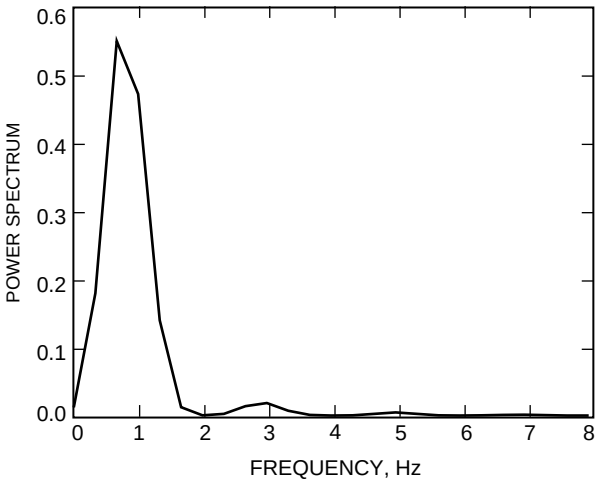

Fig. 4. The D4 mother wavelet power spectrum.

by $2^{-n/2}|\Psi_0(2^n w)|$, where $\Psi_0(w)$ is the Fourier transform of the mother wavelet. Thus, the frequency resolution changes in multiples of two. When the frequency error is small (much less than 1 Hz), then we would be able to obtain very good frequency resolution by setting a large enough value for the maximum n (i.e., the lowest frequency). However, this would be at the expense of increasing the observation window (support of the lowest-frequency wavelet). In contrast, large frequency errors (much greater than 1 Hz) require shorter observation times but provide poorer frequency resolution.

For each fixed integer n, the set $\{\psi_{n,0}, \psi_{n,\pm 1}, \cdots\}$ forms an orthonormal system, as does the set $\{\psi_{0,k}, \psi_{\pm 1,k}, \cdots\}$ for each fixed integer k. We assume that $-N_2 \leq n \leq N_1$ for some positive integers N_1 and N_2, which implies that our frequency range is $[2^{-N_1}, 2^{N_2}]$. This in turn implies a minimum observation interval of $[0, 2^{N_1}3]$. For each n, there exists a corresponding K^n_{max} such that $2^n(K^n_{max}+3) \leq 3 \times 2^{N_1}$. With these ranges for n and their corresponding K^n_{max}, we form an orthonormal set of M complex-valued wavelet functions (for resolving positive frequencies) along with their M complex conjugates (to resolve negative frequencies). This constitutes the wavelet basis set, which is orthonormal on the interval $[0, T]$, where $T = 3 \times 2^{N_1}$. The same construction applies to any wavelets of the form given in Eq. (17).

It is easily verified that the set of wavelets constructed above fits within the general framework developed in the last section. In particular, we may apply Eqs. (14) and (15) to predict the S-curve and the variance curve. Assuming a frequency range of $[-1, 1]$ Hz, we applied Eqs. (14) and (15) at different SNR [defined as $10\log(A/N_0)$ dB-Hz] levels. These results are shown in Figs. 5 and 6 in the dotted lines along with simulated S-curves and variance curves (stars) for positive frequencies only. In these figures, we used $N_1 = 7$ and $N_2 = 0$, which implies a minimum frequency estimate of $\pm 2^{-7} = \pm 0.0078$ and a maximum of ± 1. To obtain such small values, we require an observation window of length $3 \times 2^7 = 384$ seconds. For smaller values of N_1, we can still maintain the same performance for frequency offsets away from zero, but we pay the price when the frequency error is small. This is depicted in Figs. 5(b) and 6(b), where we show the S-curves and variance curves corresponding to $N_1 = 3, 4, 5$, and 7 with the SNR fixed at 10 dB-Hz. Note that the S-curves are identical in the range $[0, 1]$, with slight differences in the region ($f_e > 1$). The variance curves also are almost identical in the frequency range away from zero. Thus, for initial offsets away from zero, the performance is not affected by the window size (and, hence, we can obtain the estimate of the offset rather quickly). However, in the tracking mode, smaller observation intervals yield larger variances. Figure 7 shows a more detailed behavior of the variance curve for small f_e at a 10 dB-Hz SNR. As N_1 decreases, the variance at the origin increases because the minimum resolvable positive frequency 2^{-N_1} is sufficiently far away from zero, and as such, the presence of noise can produce a maximum projection coefficient that corresponds to any of the other frequencies in the interval [−1,1]. This is consistent with the notion that wavelets require shorter times for acquisition but longer times for tracking.

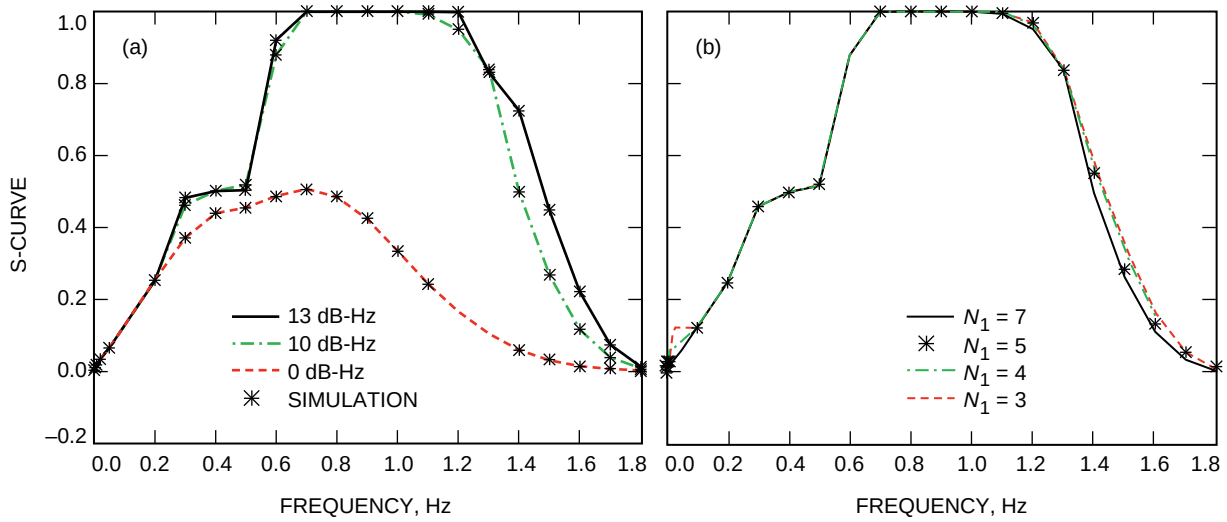

Fig. 5. S-curves for a D4 wavelet: (a) $N_1 = 7$ and (b) 10 dB-Hz.

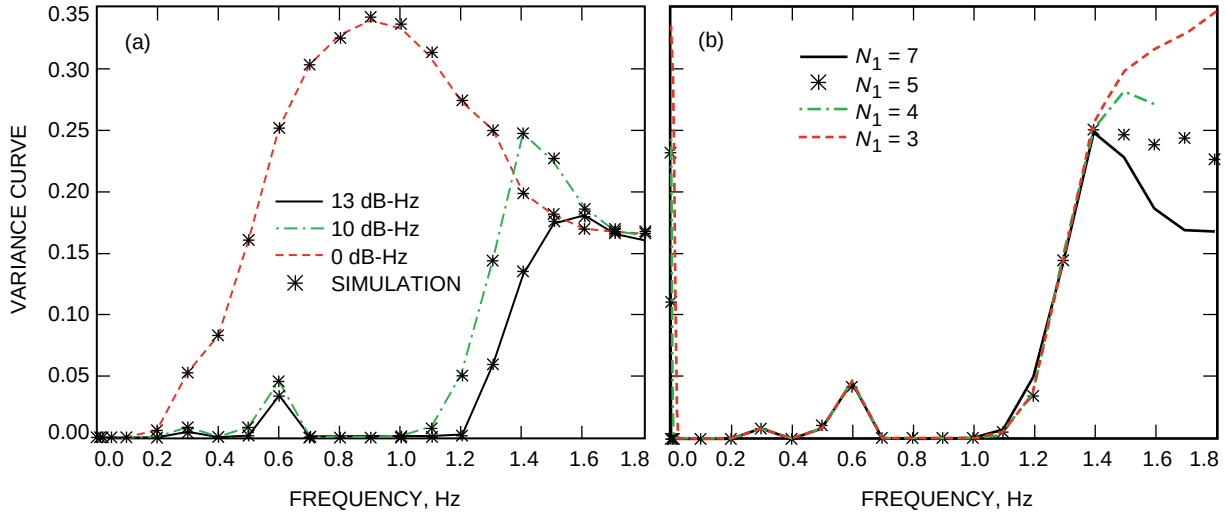

Fig. 6. Variance curves for a D4 wavelet: (a) $N_1 = 7$ and (b) 10 dB-Hz.

In order to compare the previous results with more traditional AFC loops, we now consider Fourier basis functions, which are known to be optimal in the sense of obtaining the Cramer–Roa lower bound (i.e., they represent the "matched filter") when the input frequency is constant. The basis functions $\psi_n(t)$ are given by

$$\psi_n(t) = \frac{1}{\sqrt{T}} \exp\left(2\pi j \frac{n}{T} t\right) \quad n = 0, \pm 1, \cdots, \pm M \tag{18}$$

where T is a positive integer denoting the observation interval and M is an integer multiple of T that determines the desired frequency range. One can check that this set of functions forms an orthonormal basis on the interval $[0, T]$. In Figs. 8 and 9, we show the S-curve and variance curve at a 0 db-Hz SNR and for different values of the observation interval T. Here we use different values for T and M such that the frequency range is $[-1, 1]$ Hz. As expected, the error and variance decrease with increasing

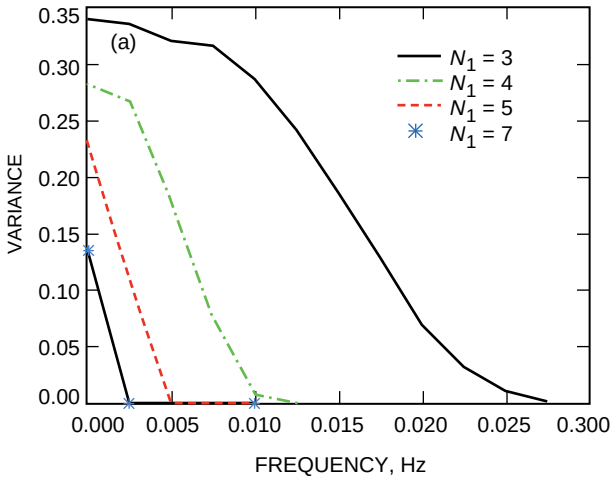

Fig. 7. Variance curves at 10 dB-Hz.

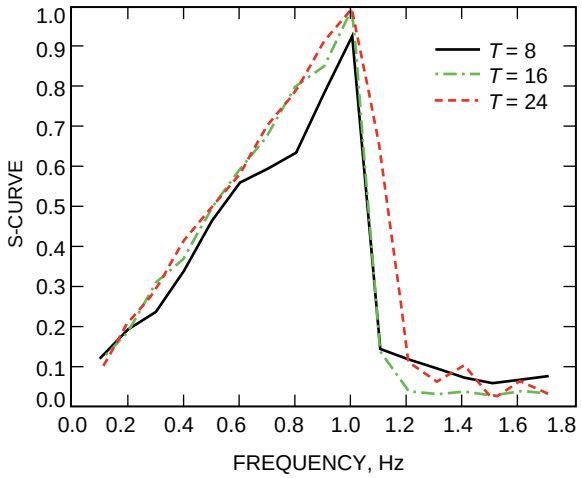

Fig. 8. S-curves for a discrete-time Fourier transform (DTFT) (0 dB-Hz).

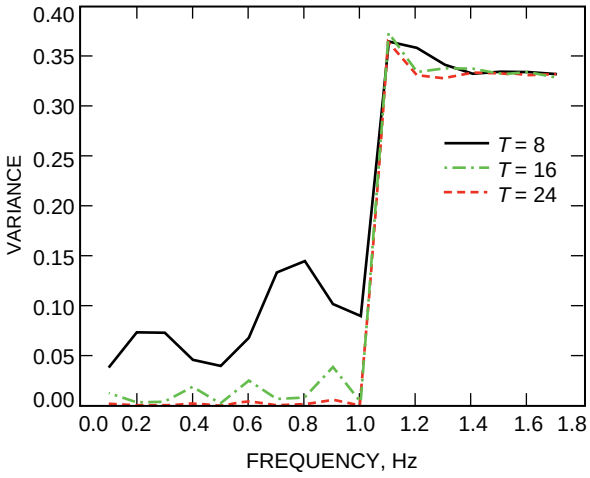

Fig. 9. Variance curves for a DTFT (0 dB-Hz).

window size at almost all frequency ranges. This is different from what was observed in the wavelet case [Fig. 6(b)]. On the other hand, by comparing the results in Fig. 9 with those obtained for the wavelets at 0 dB-Hz in Fig. 6, the clear superiority of the Fourier basis functions is evident when f_e lies in the range $[-1, 1]$. When $|f_e| > 1$, (e.g., if we lose lock and the error is outside our range), we note that the error estimate obtained using the Fourier functions immediately approaches zero (the mean value in the range $[-1, 1]$) and the variance immediately arrives at its maximum value. For the wavelets, the same qualitative behavior occurs but at a much slower pace. Thus, if the frequency offset is moderately outside the predetermined range of $[-1, 1]$, the wavelet-based AFC loop would yield a better estimate of the offset than would the Fourier-based loop.

V. Closed-Loop Performance With High Frequency Rate

In this section, we examine the performance of the AFC loops with high-dynamic input. In particular, we assume that the input frequency is of the form

$$f_c(t) = \alpha t \quad \alpha > 0 \tag{19}$$

We begin our analysis assuming no noise. We assume that in steady state the error is small enough such that linear analysis applies. In this case, we express the error estimate, $\hat{f}_e$, as

$$\hat{f}_e = S(f_e) = S_0 f_e + O(f_e^2) \tag{20}$$

where $S(f_e)$ is given in Eq. (14) and $S_0 = S'(0)$. With f_e given as in Eq. (4), the NCO linear dynamics corresponding to Eq. (5) reduce to

$$f_o(k+1) = (1 - gS_0) f_o(k) + gS_0 f_c(k) \tag{21}$$

Applying the Z-transform to Eq. (21) and using $f_c(k) = \alpha k$, the resulting Z-transform of f_e is given by

$$Z(f_e) = \frac{z-1}{z-1+gS_0} \; \frac{\alpha z}{(z-1)^2} \tag{22}$$

Applying a well-known limit theorem (see [6]) to obtain the error f_e in steady state, we obtain

$$\lim_{k\to\infty} f_e(k) = \lim_{z\to 1}(z-1)Z(f_e) = \frac{\alpha}{gS_0} = \frac{\alpha}{4B_L} \tag{23}$$

where B_L is the loop bandwidth. In the simulations to follow, we assume the input frequency given by Eq. (19). Note that, using Eq. (23), the simulations can be used to approximate B_L for the different AFC loops under consideration. Again, we begin by examining the AFC loop with Fourier basis functions. In the dashed line of Fig. 10, we show the steady-state frequency error as a function of the frequency rate α and for a fixed observation interval of $T = 3$ seconds and a loop gain of $g = 1$. The frequency resolution always is set to $[-4\alpha, 4\alpha]$, and we assume the MAP detection algorithm. As Eq. (23) suggests, the steady-state error increases with increasing values of the rate α, but for $\alpha > 3.5$, the loop breaks down and the error grows without bound. From the same plot, the inferred value for the loop bandwidth B_L [using Eq. (23)] is $B_L = 0.2726$ Hz.

We now consider the AFC loop with the wavelet basis functions. Again, we assume $T = 3$ seconds and $g = 1$, which implies that the smallest frequency that $\hat{f}_e$ can take on is 1 Hz. The maximum frequency

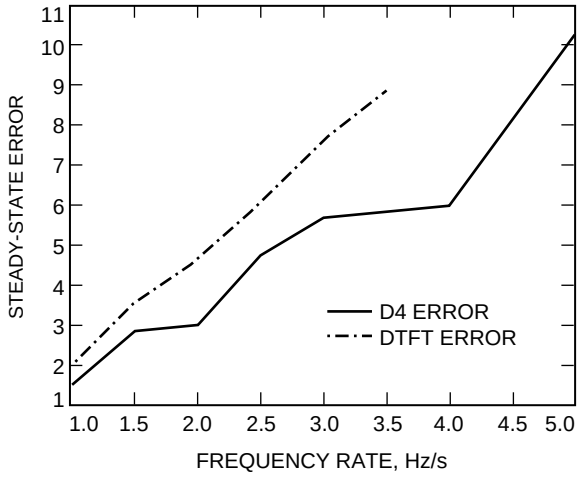

Fig. 10. Steady-state error versus frequency rate.

that $\hat{f}_e$ can take on (2^{N_2} for some integer $N_2 > 0$) will also depend on α, and in the absence of noise, this choice does not affect the steady-state error provided it is large enough to resolve the maximum frequency error within a single observation interval. The solid line in Fig. 10 shows the steady-state error as a function of α. Note that the wavelet-based AFC loop achieves a smaller steady-state error than does the Fourier-based loop. More importantly, the wavelet-based loop continues to track for a much larger range for α. The inferred value for the wavelet-based loop bandwidth is $B_L = 0.3776$ Hz.

Figure 11 is similar to Fig. 10 except now the SNR is 20 dB-Hz. Again, we observe the same behavior for the steady-state error, with the Fourier-based loop breaking down near $\alpha = 3$. Figure 12 shows the corresponding steady-state variance for both loops. The D4 loop obtains a lower steady-state variance up to $\alpha = 2$ Hz/s, then the variance grows by a significant amount, and then it goes down again. This nonlinear behavior of the variance can be explained by considering the frequency spacing for wavelets for frequencies much larger than 1 Hz. When the true frequency range is near 9 Hz (i.e., $\alpha = 3$ in a 3-second window), the two nearest frequencies are at 8 and 16 Hz. Thus, a misdetection of the true frequency can cause a large variance in an ensemble of estimates. We note that increasing the SNR to 30 dB-Hz reduced the steady-state error variance at $\alpha = 3$ from 7.866 to 4.137 Hz^2, and the variance at $\alpha = 5$ from 2.65 to 1.133 Hz^2. We expect that similar highly nonlinear behavior will hold for any wavelet since the frequency spacing also will be logarithmic. This is not the case for the Fourier-based loop, where the frequency spacing for large frequencies is the same as it is for small frequencies. However, although the variance of the error does not grow very much as α increases in the Fourier-based loop, the allowable frequency rate range for which the Fourier loop can track is much smaller than that for the wavelet-based loop. This same behavior is seen in Figs. 13 and 14, which show the steady-state error and corresponding variance of the error when the observation window is extended to $T = 6$ seconds. Again, the SNR is 20 dB-Hz. By comparing the steady-state errors (Fig. 11 for $T = 3$ and Fig. 13 for $T = 6$), we see that the error increased by a factor of approximately two. Thus, for example, the Fourier-based loop cannot track when the frequency rate is greater than 1.5 Hz/s when $T = 6$, and 3.0 Hz/s when $T = 3$.

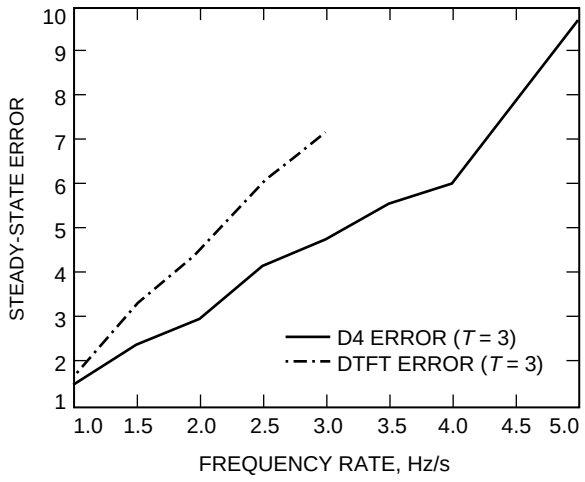

Fig. 11. Steady-state error (20 dB-Hz).

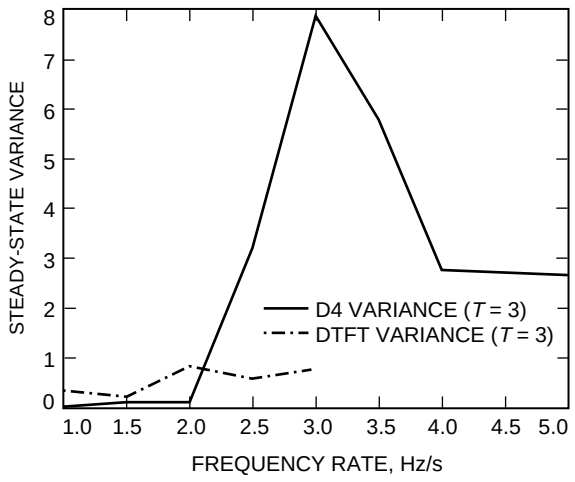

Fig. 12. Steady-state variance (20 dB-Hz).

VI. Conclusion

The main results of this study can be summarized as follows: When the input frequency is constant or very slowly varying, the S-curves and variance curves illustrate that the Fourier-based loop will perform better than the wavelet-based loop for any fixed observation interval. In fact, tracking a constant frequency using a wavelet-based loop will require an unnecessarily large observation interval. Therefore, using wavelets when the frequency is constant offers no advantages. On the other hand, when the signal

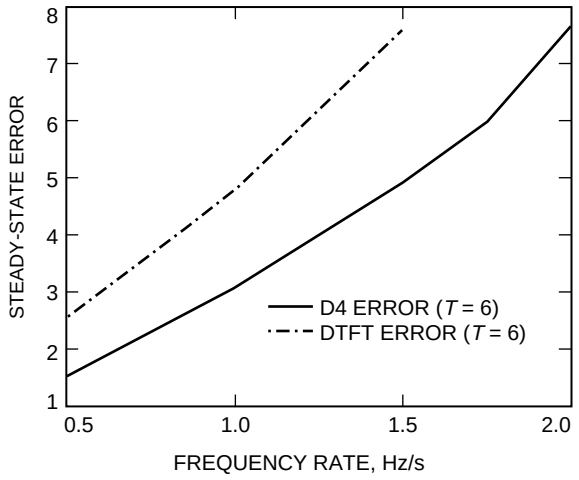

Fig. 13. Steady-state error (20 dB-Hz).

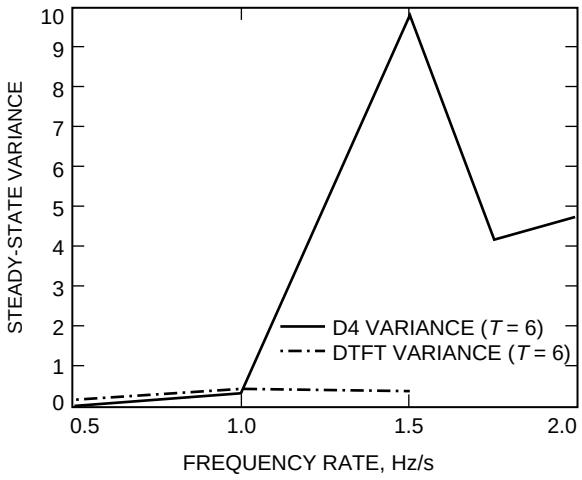

Fig. 14. Steady-state variance (20 dB-Hz).

is undergoing high dynamics, the wavelet-based loop performs better than does the Fourier-based loop. Our results indicate that if the frequency rate is large enough (depending on observation interval and the SNR), then the Fourier-based loop ceases to track while the wavelet-based loop continues to track. This suggests that a wavelet-based loop can be considered in future applications where the frequency dynamics are significant and unpredictable. What we did not discuss in this article are improvements to the MAP detection algorithm. This area will need more investigation. Also, we did not discuss the problem of frequency-rate estimation. Our initial investigation has shown that wavelets can also be promising for estimating the frequency rate. This will also be considered in detail in the near future. However, other families of wavelets, as well as other Daubechies wavelets, will have to be tested and their performances analyzed before we can truly assess the benefit of using wavelets for frequency tracking.

References

[1] F. Natali, "AFC Tracking Algorithms," *IEEE Trans. on Communications*, vol. COM-32, no. 8, pp. 935–947, August 1984.

[2] K. Yokogawa, S. Hara, and N. Morinaga, *An Automatic Frequency Control Method Using Wavelet Transform*, IEICE Technical Report RCS-11, pp. 77–84, 1993-05.

[3] A. Papoulis, *Probability, Random Variables, and Stochastic Processes*, New York: McGraw Hill, 1984.

[4] I. Daubechies, *Ten Lectures on Wavelets*, SIAM, 1992.

[5] G. Strang and T. Nguyen, *Wavelets and Filter Banks*, Wellesley, Massachusetts: Wellesley–Cambridge Press, 1996.

[6] K. Shlomo and W. Byatt, *Mathematical Methods in Continuous and Discrete Systems*, New York: Holt, Rinehart and Winston, 1982.